# Chemical Abundances in Carbon-enhanced Metal-poor Stars

A Senior Honors Thesis

Presented in Partial Fulfillment of the Requirements for graduation *with research distinction* in Astronomy in the undergraduate colleges of The Ohio State University

by

Anna Kwa

The Ohio State University

May 2011

Project Adviser: Professor Jennifer Johnson, Department of Astronomy

## ABSTRACT

Metal-poor stars in the Galactic halo were born during the first few generations following the Big Bang, and thus provide key insights regarding conditions in the early Universe. Carbon-enhanced metal-poor (CEMP) stars, a subset of this population, are of even further interest because of their peculiar elemental abundance patterns. We studied high-resolution spectra of ten CEMP stars to learn more about the sources of their carbon excess, and now have preliminary abundances for up to 29 elements in our sample. Carbon enhancement in the stellar atmospheres was taken into consideration when conducting the abundance analysis, but did not appear to have a significant effect on derived abundances. Comparison of heavy element abundance ratios to the solar system pattern will be used to study nucleosynthesis at extremely low metallicities.


## 1. Introduction

### 1.1. Metal-poor stars

In the field of astronomy, the term 'metal' is used to refer to all elements heavier than hydrogen and helium. The atomic number Z of an element is the number of protons in an atomcs nucleus, with higher Z's corresponding to heavier elements. The three lightest elements- hydrogen, helium, and lithium- were formed during the first minutes following the Big Bang, when conditions had cooled sufficiently to allow for stable protons and neutrons to form but were hot and dense enough to fuse the elements H-2, He-3, He-4, Li-6, and Li-7. This process, known as Big Bang nucleosynthesis, lasted only about seventeen minutes before the Universe cooled to a temperature too low for nuclear fusion to produce heavier elements. The first stars in the Universe formed out of gas clouds of these light elements and were therefore metal-free. Metals heavier than lithium are synthesized through nuclear fusion in stellar interiors and supernovae and dispersed into the interstellar medium. Stars formed out of gas that had been enriched with metals from previous generations. Thus, there is a general age-metallicity relation, with subsequent younger generations of stars having increasing metallicities.

### 1.2. Metal-poor stars and carbon enhancement

Metal-poor stars are found in the Milky Way halo, a spherical distribution of stars that formed out of clumps of old stars. Although the frequency of metal-poor stars in the halo is high, it is very diffuse, making these stars extremely rare in the solar neighborhood- only about 0.1% of stars within a few kiloparsecs of the Sun have [Fe/H]<-2.0[1]. Despite the difficulty involved in finding metal-poor stars, much effort has been expended in searching for them. Unlike high-redshift galaxies that are approximately the same age but are hundreds of megaparsecs away, metal-poor stars are artifacts of the young Universe that are easily observed within the solar neighborhood, providing that they can be located. Their usefulness in the study of near-field cosmology has been the motivation behind multiple surveys to find them in the galactic halo.

Most of these stars lie within a few hundred parsecs of the Sun and were found using spectroscopic surveys, notably the HK and Hamburg-ESO surveys. Candidate stars are found in the initial wide-field, low-resolution spectroscopic surveys, and then follow-up spectra is taken at moderate resolution to confirm that they are indeed metal-poor. A follow-up study of metal-poor candidates from the HK survey yielded the very interesting finding that many metal-poor stars also show strong absorption in molecular carbon bands (Beers, Preston, & Schectman 1992). Carbon levels are considered to be enhanced if [C/Fe]>1.0. The fraction of metal-poor stars that are also carbon-enhanced is much higher than the fraction of solar-metallicity stars exhibiting carbon enhancement. Approximately 20% of metal-poor stars with [Fe/H]<-2.0 are carbon-enhanced, with this fraction increasing with decreasing metallicity (Lucatello et al. 2006).

Carbon-enhanced metal-poor (CEMP) stars raise many interesting questions. Their luminosities are low enough that they cannot be asymptotic giant branch (AGB) stars, which dredge up carbon from the core to the surface, where it can be detected. Unless these stars were able to dredge up carbon to their surfaces before reaching the AGB phase, they must either have formed with their excess carbon or have been polluted by carbon produced extrinsically from some outside source. The increasing fraction of CEMP stars at the lowest metallicities suggests that for whatever reason, the mechanism(s) responsible for increasing their carbon content occurred more frequently and/or more efficiently in the early Universe.

[1]See appendix 1.1 for an explanation of the notation used to describe metallicity

In addition to enhanced levels of carbon, almost all CEMP stars also show enhancements in their neutron-capture element abundances. Neutron-capture elements are synthesized via either the s- or r- processes. The slow, or s-process, occurs at relatively low neutron densities in the interiors of asymptotic giant branch (AGB) stars. The rapid, or r-process, occurs at high neutron densities in explosive environments, such as core-collapse supernovae or neutron star mergers. Both processes produce heavy neutron-capture elements in very specific ratios. By measuring these relative abundances in a star, it is possible to infer which neutron-capture process was responsible for producing the bulk of its heavy elements. A wide diversity of r- and s-process elemental abundances have been measured in CEMP stars, leading to further classification as CEMP-s, -r, -r/s, or no stars based on whether or not they exhibit enhancements of elements produced in one, both, or none of the two processes.

Since most theories assume that CEMP stars received their carbon and heavy element enhancements at the same time, these subcategories suggest the existence of multiple carbon sources. Various enrichment scenarios have been put forth to explain the observed chemical abundances of different types of CEMP stars. CEMP-s stars are the most common and perhaps the most well-understood of the CEMP subclasses; about 80% of CEMP stars are s-process enhanced. They are believed to be low-mass members of a binary system that were polluted by mass transfer from a companion AGB star. At some time in the past, the more massive companion star underwent AGB evolution and synthesized s-process elements in its core. During this stage, material from the core (including carbon) was dredged up to the surface and blown off in stellar winds. Material from the AGB star was accreted by the smaller companion and polluted it with the excess carbon and heavy elements that are observed today. The AGB companion has since evolved into a faint white dwarf, which is why only the CEMP star is observed today. This theory is easily tested by taking radial velocity measurements to determine binary membership. $\sim$68% of CEMP-s stars are confirmed binaries, which is statistically compatible with a binary frequency of 100% after correcting for factors such as inclination and long periods (Lucatello et al. 2005).

The origin of the remaining classes of CEMP stars remains a topic still open for debate. CEMP-r/s stars constitute most of the remainder of the CEMP population after the s-enhanced stars. It has been proposed that they received their s-process enhancement in the same manner as CEMP-s stars, but received their r-process enhancements separately, either from formation out of a gas cloud polluted by a nearby supernova (Ivans et al. 2005) or from their companion exploding as an electron-capture supernova after its AGB phase (Wanajo

et al. 2005). Lugaro et al. (2009) hypothesize that the r- enhancement might have been produced in a neutron superburst in the companion star in the dual core flash prior to its AGB phase, and accreted onto the CEMP star at the same time as the s-process material.

CEMP-r and no stars, which show little to no s-process enhancement, may have formed out of carbon-enriched gas clouds (Beers & Christlieb 2005), or may have dredged up carbon from their core to their surface by some mechanism that only occurs at extremely low metallicities (Fujimoto et al. 2000). On the other hand, it has been proposed that the binary mass transfer hypothesis could explain all classes of CEMP stars if the efficiency of the s-process varied at very low metallicities (Cohen et al. 2006, Busso et al. 1999). In order to test these theories, more detailed heavy element abundance patterns are needed for a larger number of CEMP stars.

### 1.3. Motivation

Studies of detailed chemical abundances in CEMP stars are therefore a unique way to study stellar evolution and nucleosynthesis using some of the oldest stars known. Because it is possible to infer how CEMP stars were polluted and how the elements they were polluted with were synthesized, they can be considered a 'fossil record of the early Universe. However, as previously mentioned, metal-poor stars are rare and thus the number of CEMP stars for which detailed chemical abundances have been measured is small. The goal of this project is to increase this dataset and obtain chemical abundances for a sample of CEMP stars. Some of the elements studied in this project have absorption lines that are difficult to resolve; consequently, there are relatively few stars of which sufficiently high-resolution spectra have been taken to determine these elemental abundances. Measuring a large number of elements in CEMP stars will provide even more information that can be used to answer the many questions that they raise.

## 2. Observations and data reduction

Observations of the target stars were taken at the Keck Observatory in Mauna Kea, Hawaii. Targets were selected with the criteria that they 1) were known through previous spectroscopic studies to have high [C/Fe] and 2) had high enough temperatures that con-

vection would not have depleted lithium from the surface (so that it might be possible to measure Li abundances.) High-resolution spectra were obtained using the High-resolution Echelle Spectrometer (HIRES) (Vogt et al. 1994) and reduced using the standard HIRES calibration (Barlow 2002). Resolution was ∼45,000 and signal to noise at 5800 Åwas greater than ∼100, and greater than ∼125 in most cases.

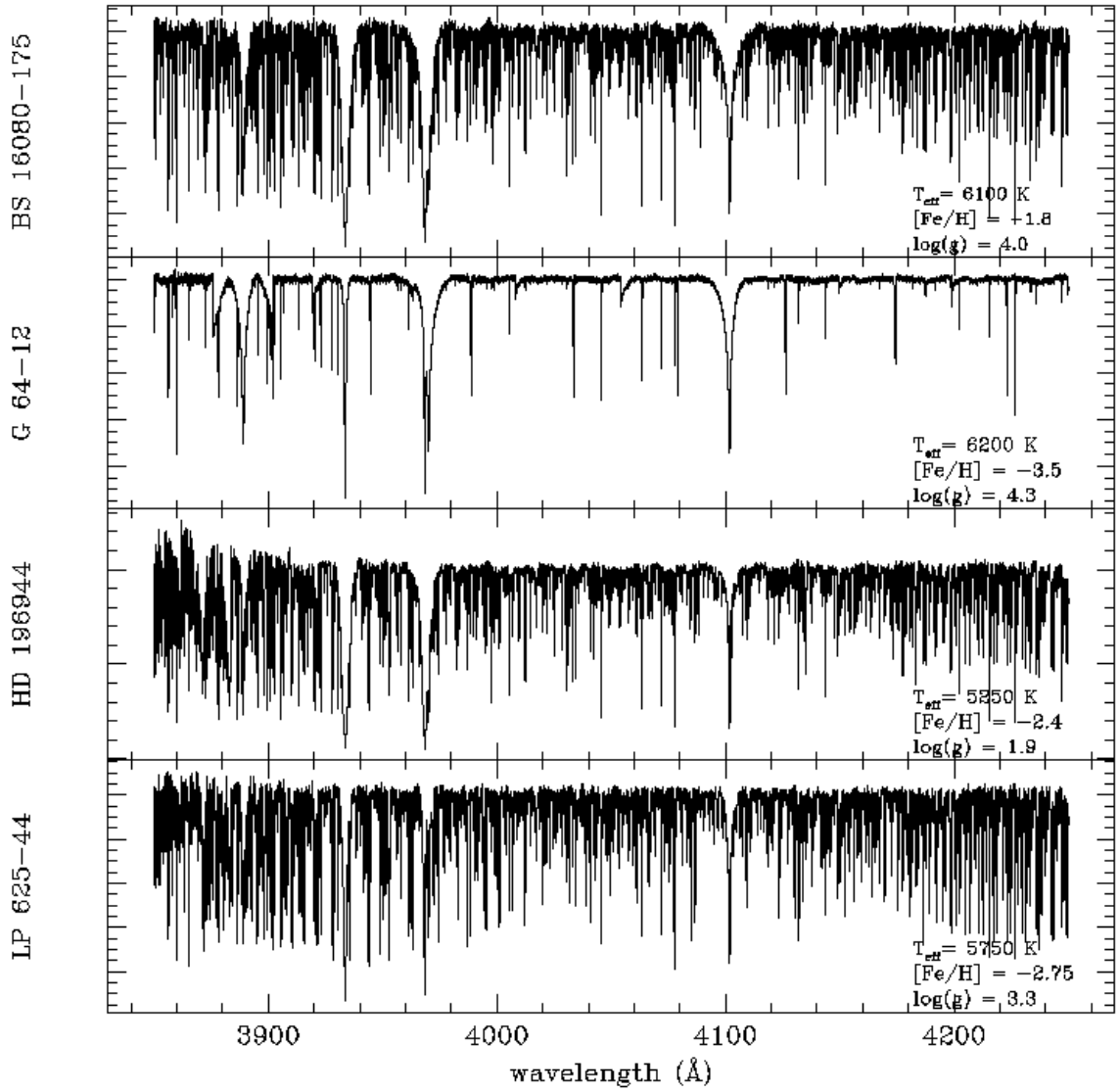


Fig. 1.—Examples of spectra from metal-poor stars in this study. Note that G 64-12, the star with the highest temperature and lowest metallicity shown, has markedly fewer absorption lines in its spectrum.

## 3. Data analysis

Elemental abundances were derived using one of two methods. If possible, the equivalent widths of spectral absorption features were measured (see appendix 1.2). The abundance analysis code Turbospectrum was used to compute chemical abundances based on the spectral line strengths and the appropriate stellar parameters. For some elements, however, equivalent widths of an elements absorption lines could not be measured; in these cases synthetic spectra were generated by varying the abundance of the element in question and the adopted abundance was chosen to be the value that produced the best fit to the observed spectrum.

### 3.1. Equivalent width measurements

Calculation of abundance values from equivalent widths requires a knowledge of which spectral features correspond to which element, and also the oscillator strengths and excitation potentials for each individual line. For this project, a line list containing this information from a number of sources was readily available. Lines were removed from the list if they proved to be blended with another spectral line when checked in the solar spectrum atlas (Moore 1966).

### 3.2. Stellar parameters

Equivalent widths are dependent on not only the abundance and atomic parameters, but also the temperature ($T_{eff}$), surface gravity (log g), microturbulence (vt), and metallicity (Z) of the star. It is therefore necessary to know these stellar parameters when performing abundance calculations. Parameters were determined by placing the following constraints on Fe I and Fe II equivalent widths:

1. Effective temperature: Excitation equilibrium had to be satisfied, i.e. the value of [Fe/H] for any line should be constant irregardless of its excitation potential.

2. Surface gravity: The values of [Fe/H] calculated from Fe I and Fe II lines must agree.

3. Microturbulence: All equivalent widths should give the same [Fe/H].

4. Metallicity: The value of [Fe/H] that satisfies all the above conditions is used in the stellar models.

This project used model atmospheres from the MARCS grid (Gustafsson et al. 2008). An initial guess as to the stellar parameters was made and a model with these values was interpolated from the grid. Turbospectrum would then calculate chemical abundances using this model and the measured equivalent widths by solving the equations of radiative transfer and the Saha and Boltzmann equations. The resulting values of [Fe/H] from the iron lines were examined graphically (Fig. 2) and appropriate adjustments were made to the parameters for the stellar atmosphere. This process was reiterated using the new parameters until the previously mentioned constraints were satisfied and the final abundances were calculated in Turbospectrum.

### 3.3. Comparison with literature equivalent widths and temperatures

As the stars in the sample had all been previously studied (but not in as much detail), their stellar parameters could be compared to existing values in published literature. Unlike the effective temperatures used in this project, which were derived spectroscopically by demanding excitation equilibrium of the iron lines, almost all the temperatures in the literature had been determined photometrically using colors. Surface gravity and microturbulence were found in much the same way as in this project, except that the effective temperature of the model atmospheres was fixed at the photometric value. Literature values for surface gravity and microturbulence also differed from those measured in this study (Table 1). Published colors were used to calculate photometric temperatures, with reddening taken into account; these generally agreed with the photometric temperatures from the literature (Ramirez & Melendez 2005). In most cases, the effective temperatures and metallicities from this project were lower than the literature values. If iron equivalent widths were available in the literature, they were compared to those from this study.

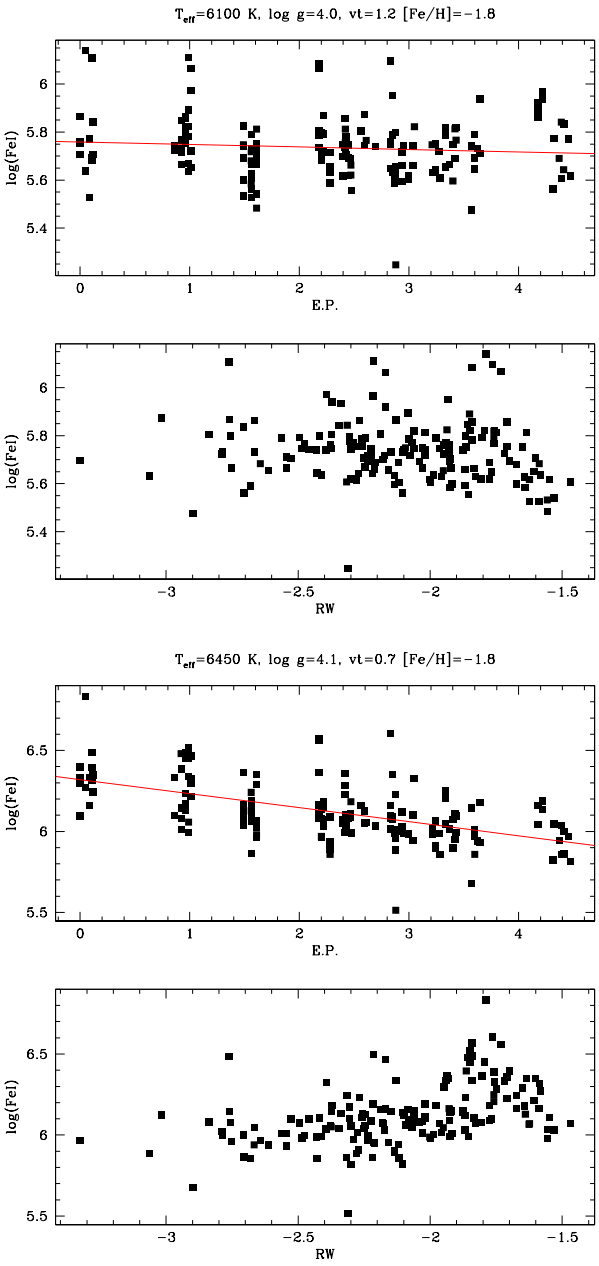


Fig. 2.—Excitation potential (top) and equivalent width (bottom) vs. [Fe/H] for each individual line measured in BS 16080-175. Figure 2a shows the plots for the adopted temperature, surface gravity, and microturbulence; these were the stellar parameters that gave the most constant values of [Fe/H] for every excitation potential and equivalent width. Figure 2b is an example of a set of stellar parameters that result in inconsistent values of [Fe/H]. The red line is the best linear fit to excitation potential vs. [Fe/H]. Ideally, it would have slope m=0 for constant [Fe/H]; often, after all other constraints were satisfied the slope would be within +/- .01.

| Object | $T_{eff,meas}(K)$ | $T_{eff,lit}(K)$ | log $g_{meas}$ | log $g_{lit}$ | $[Fe/H]_{meas}$ | $[Fe/H]_{lit}$ |
|---|---|---|---|---|---|---|
| BS 16080-175 | 6100 | 6240 | 4.0 | 3.7 | -1.8 | -1.86 |
| CS 22877-001 | 4750 | 5100 | 1.6 | 2.2 | -3.3 | -2.72 |
| G 64-12 | 6200 | 6295 | 4.3 | 4.4 | -3.5 | -3.37 |
| HD 196944 | 5250 | 5250 | 1.9 | 1.7 | -2.4 | -2.19 |
| HE 1001-0243 | 5100 | 5000 | 2.4 | 2.0 | -3.2 | -2.88 |
| HE 1005-1439 | 5200 | 5000 | 2.5 | 1.9 | -3.0 | -3.17 |
| HE 1012-1540 | 5100 | 5620 | 4.0 | 3.4 | -4.15 | -3.50 |
| HE 1150-0428 | 5300 | 5200 | 3.2 | 2.6 | -3.4 | -3.37 |
| HE 1419-1324 | 4700 | 4900 | 1.1 | 1.8 | -3.5 | -3.05 |
| LP 625-44 | 5750 | 5500 | 3.3 | 2.8 | -2.75 | -2.71 |

Table 1:Stellar parameters and comparison to literature values

#### *3.3.1. LP 625-44*

Of particular interest was the star LP 625-44, as it was probably the most well-studied of the stars in the sample and there were relatively large discrepancies with stellar parameters derived in previous studies ($\Delta T_{eff} = 250K$,$\Delta$ log g = 0.5). To check which effective temperature was more accurate, the hydrogen H-$\beta$ line was synthesized using both temperatures to see which synthetic spectrum best replicated the observed line. The photometric temperature agreed better with the temperature derived from hydrogen line fits if a lower reddening value was adopted, while it agreed better with the spectroscopic temperature if a higher reddening value was adopted. Equivalent widths were compared to existing measurements by Aoki et al. (2002) and Norris et al. (1997). The equivalent widths from this study tended to be lower than those measured by Norris et al. (Fig. 3), but the scatter was more even compared to the widths from Aoki et al. (Fig. 4). Stellar parameters were rederived using Aoki et al.s equivalent widths, but there was still disagreement with the measurements from this study. The issue of which set of parameters is more accurate is still to be resolved.

### 3.4. Synthesized spectra

If absorption lines were blended with those of another element, synthesizing and fitting a spectrum was the preferred method of measuring abundances. Before synthesizing lines for

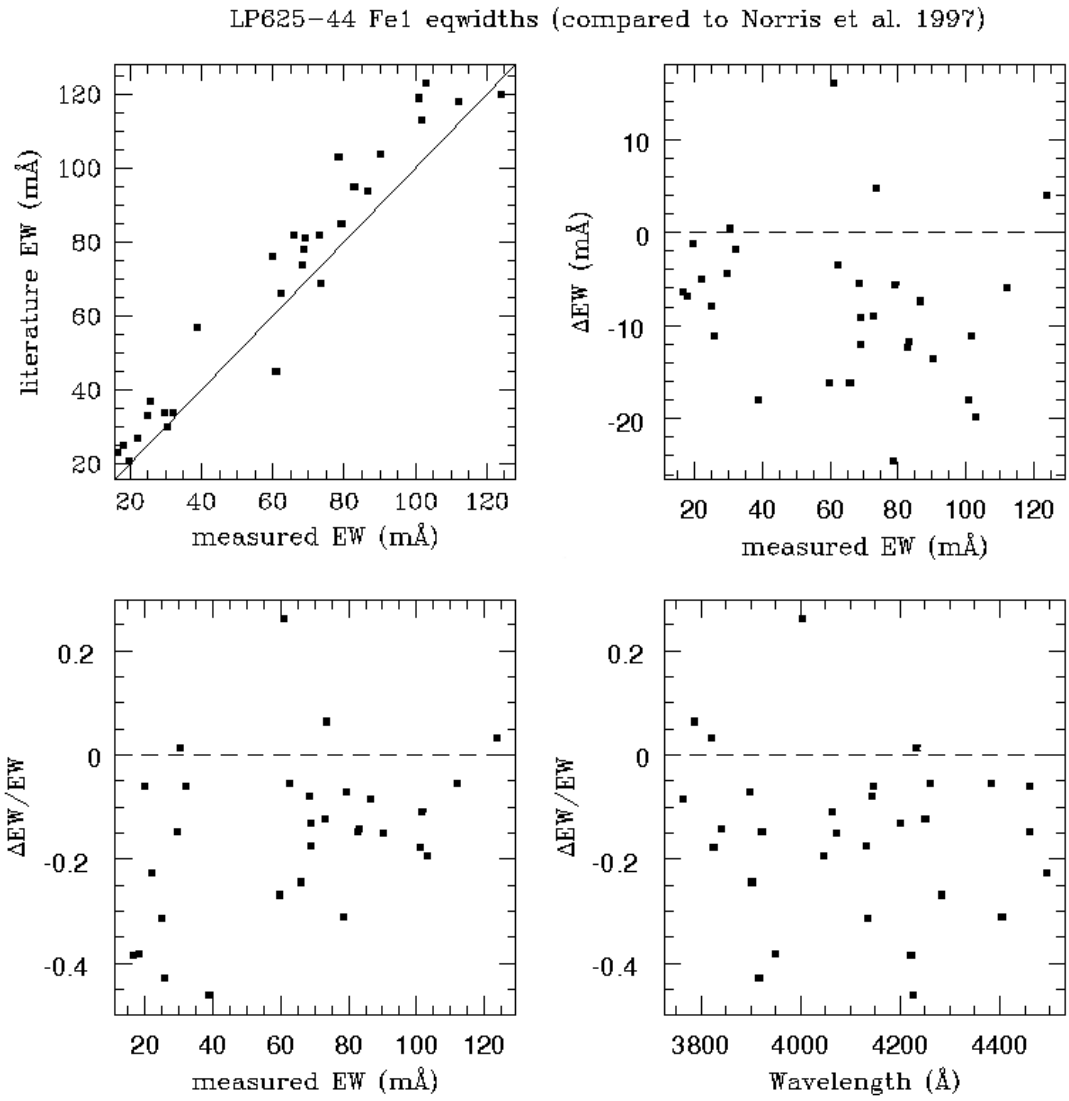


Fig. 3.—Comparison to equivalent widths from Norris et al. 1997

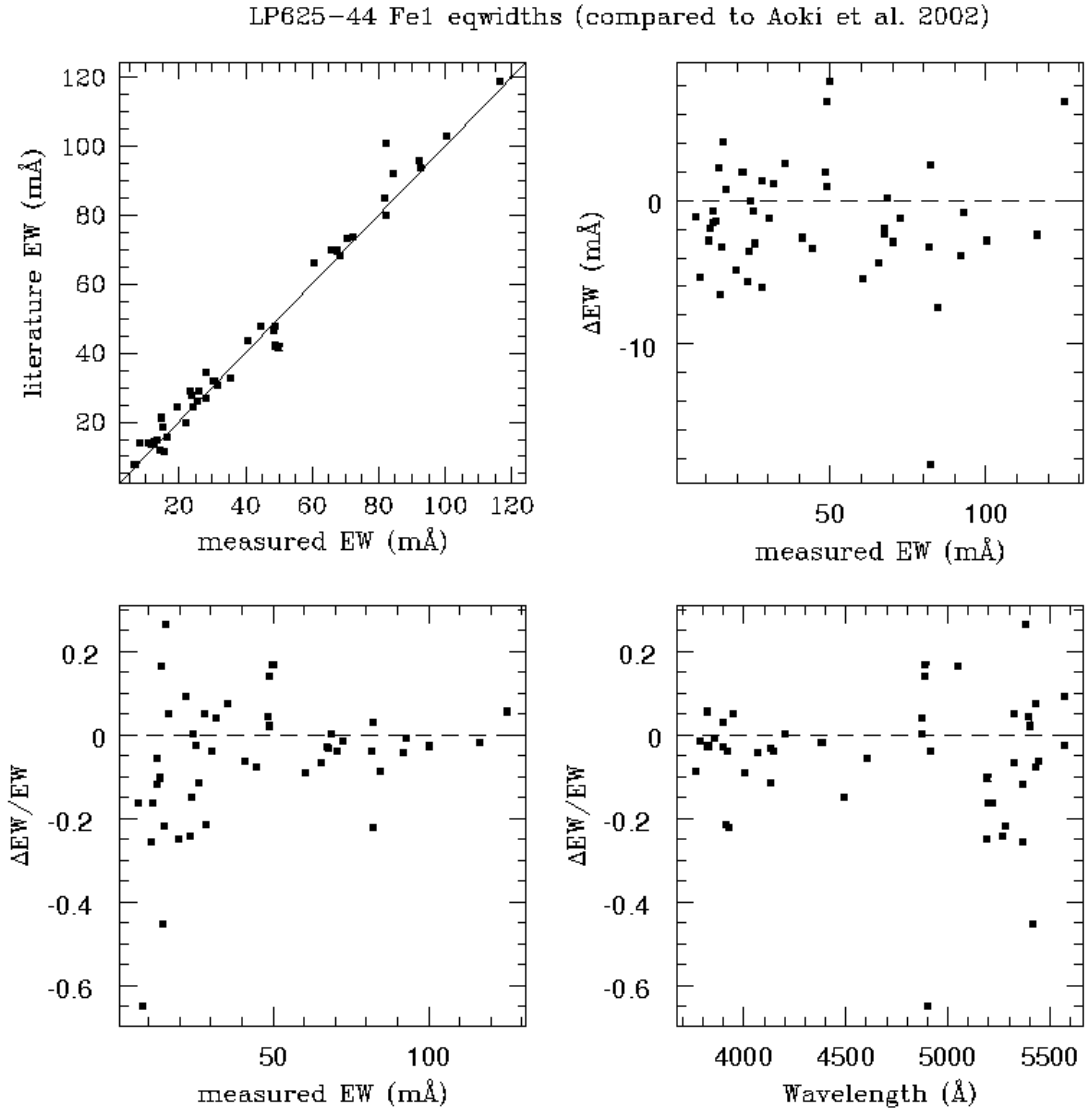


Fig. 4.—Comparison to equivalent widths from Aoki et al. 2002

heavy elements, the carbon, nitrogen, and oxygen abundances and the carbon-12/carbon-13 ratio had to be set for Turbospectrum. Many heavy element lines lay on top of these features, therefore the levels of C, N, and O must be set before attempting to synthesize these blended lines.

The only visible oxygen features were the 7774 Åtriplet and in some cases only one or two of the triplet lines were visible. These were used to determine log$\epsilon$(O). Since these stars were all carbon-enhanced, there was no problem finding many carbon features to fit a synthetic spectrum to. The exception was the star G 64-12, for which the strong molecular CH bands around 4300 Åwere used to fit the spectra[2]. The only nitrogen features visible were the CN lines around 3880 Å. For some stars, nitrogen was not strong enough to be measured; the value of [C/N] was set to zero in these cases. Likewise, the solar value of 80 for the C12/C13 ratio was adopted if no features were visible.

Heavy element lines were then synthesized for a range of abundances and plotted over the observed spectrum. Preliminary abundances were found by selecting the spectra 'by eye' that most closely resembled the absorption feature. The next step in determining the final abundances is to calculate the $\chi^2$ value for each synthetic spectrum and fitting a quadratic to the $\chi^2$'s. The best-fit value for each elemental abundance is that which minimizes $\chi^2$. This is still a work in progress, but early abundances from $\chi^2$ fitting agree well with the preliminary abundances found 'by eye.' This is not too surprising, considering that a 0.1 dex change in the log$\epsilon$ abundance produces a quite obvious change in the depth of the synthesized absorption line (Fig. 5).

Measured heavy element abundances are given in section 5.1. In addition, section 5.3 contains lithium abundances or upper limits when lithium could not be measured.

[2]The measured value of [C/Fe] for G 64-12 was 0.87, slightly less than what would technically define as 'carbon-enhanced'

### 3.5. Modeling carbon enhancement

The initial model atmospheres used to derive chemical abundances were created without taking the carbon enhancements into account. The high levels of carbon in these stars could have significant effects on the temperature structure of their atmospheres, which in turn could affect the abundance calculations. New model atmospheres were created, this time including the carbon, nitrogen, and oxygen abundances found using synthetic spectra. The abundance analysis was reiterated using these models, but introducing carbon into the atmospheres did not appear to have any significant effect. The new models resulted in changes of only 0.01 - 0.05 dex in the chemical abundances (see section 5.2).

## 4. Results and discussion

The relative abundances of the heavy elements in CEMP stars are the key to answering many of the questions that surround them. How did the levels of these elements in CEMP stars become enhanced? Did nucleosynthesis via the r- and s- processes occur differently in low-metallicity environments (i.e. the early Universe)?

Once measured, the relative abundances of heavy elements in a CEMP star may be compared to solar system abundances. Of interest are the relative abundances, not the absolute abundances, of these elements. The r- and s- processes synthesize neutron-capture elements in specific proportions; by comparing ratios such as [Ba/Eu] one can infer which process created most of the heavy elements in the star. A CEMP-r or CEMP-s star will generally follow the respective r- or s- process pattern of abundance ratios, but could show deviations from the exact solar pattern. These deviations are of interest because they might be due to nucleosynthesis in the past differing from our knowledge of how it occurs in the present-day Universe. In particular, the efficiency of the s-process in AGB stars might be affected at extremely low metallicities.

Fig. 6, 7, and 8 show heavy element abundance patterns that are reasonably consistent with s-process nucleosynthesis, while Fig. 9 shows a star that would be classified as a CEMP-r/s star. Note that in BS 16080-175 and HD 196944, the elements with Z $\sim$ 55  60 closely track the solar s-process, those with Z<55 are generally below the s-process line, and those with Z > 60 lie above it. Abundances of Pb, the heaviest element measured, lie well above

the predicted solar s-process. HD 196944 has a Pb abundance that is ∼0.4 dex greater than that of BS 16080-175 (when normalized to Ba) , while its has [Fe/H] ∼0.6 dex lower. These observations are consistent with predictions that the s-process in low-metallicity stars should produce a higher proportion of the higher Z elements and a lower proportion of lower Z elements compared to the s-process at solar metallicity (Goriely  Mowlavi 2000). Metal-poor AGB stars would have lower iron nuclei seed to neutron ratios due to their low iron abundances; this higher number of neutrons per seed nuclei would tend to produce the heavier elements rather than the lighter ones. However, this is not observed in the star LP 625-44.

Future work still remains in performing the $\chi^2$ fitting to the synthetic spectra and completing the error analysis, hence the lack of error bars on the following figures.

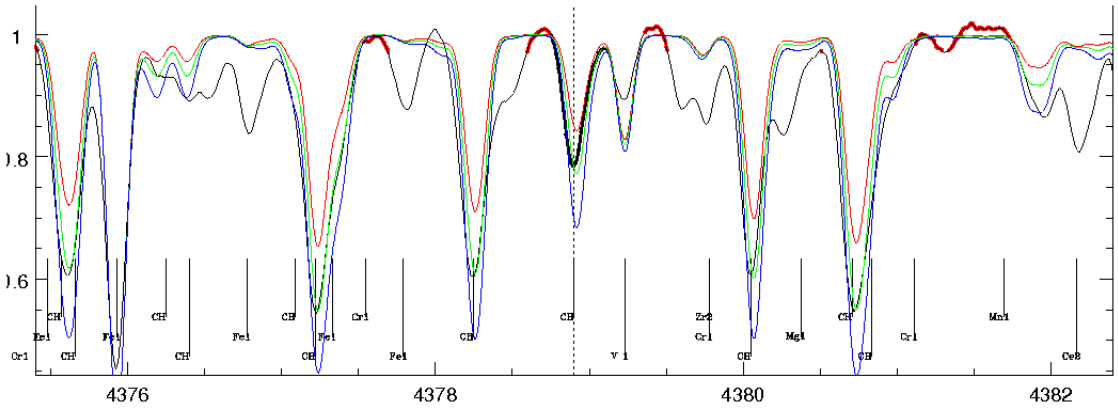


Fig. 5.—Synthetic spectrum generated using varying carbon abundances. The colored lines represent differences of 0.2 dex.

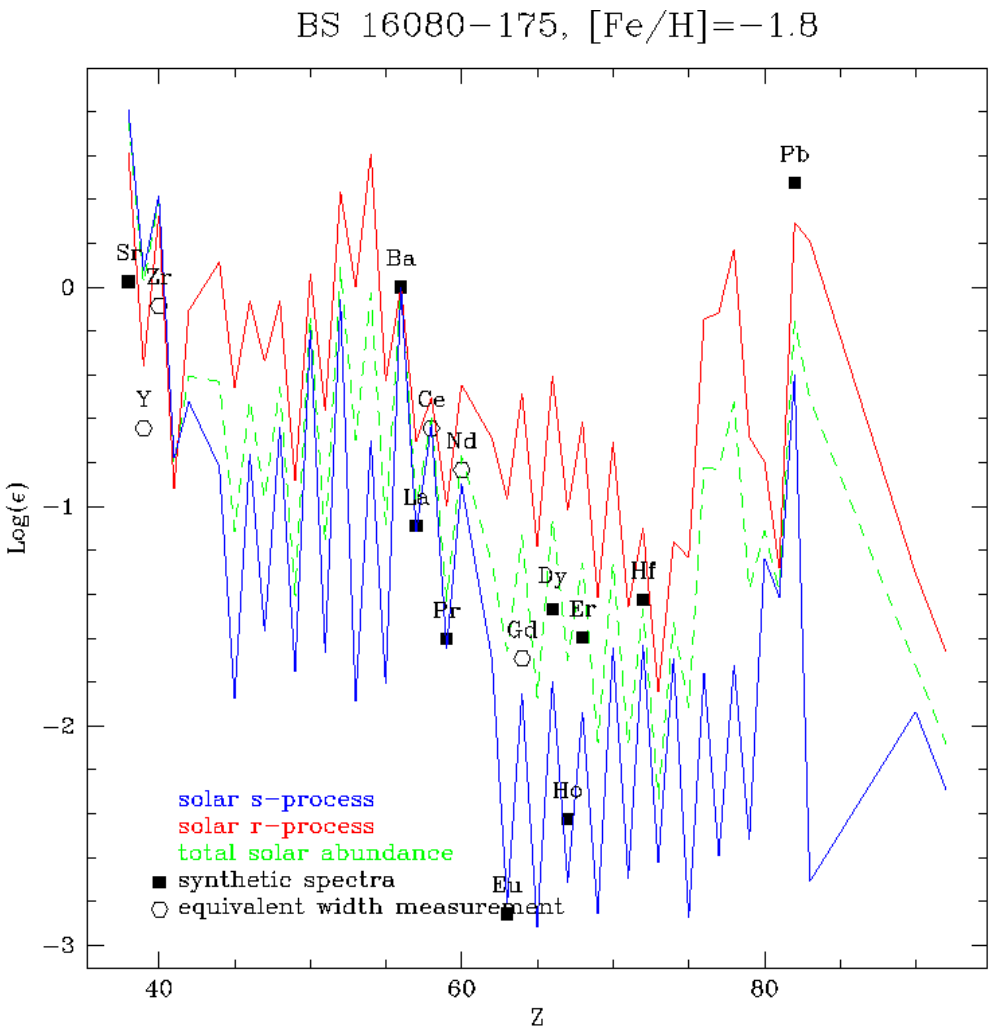


Fig. 6.—Scaled abundances in BS16080-175

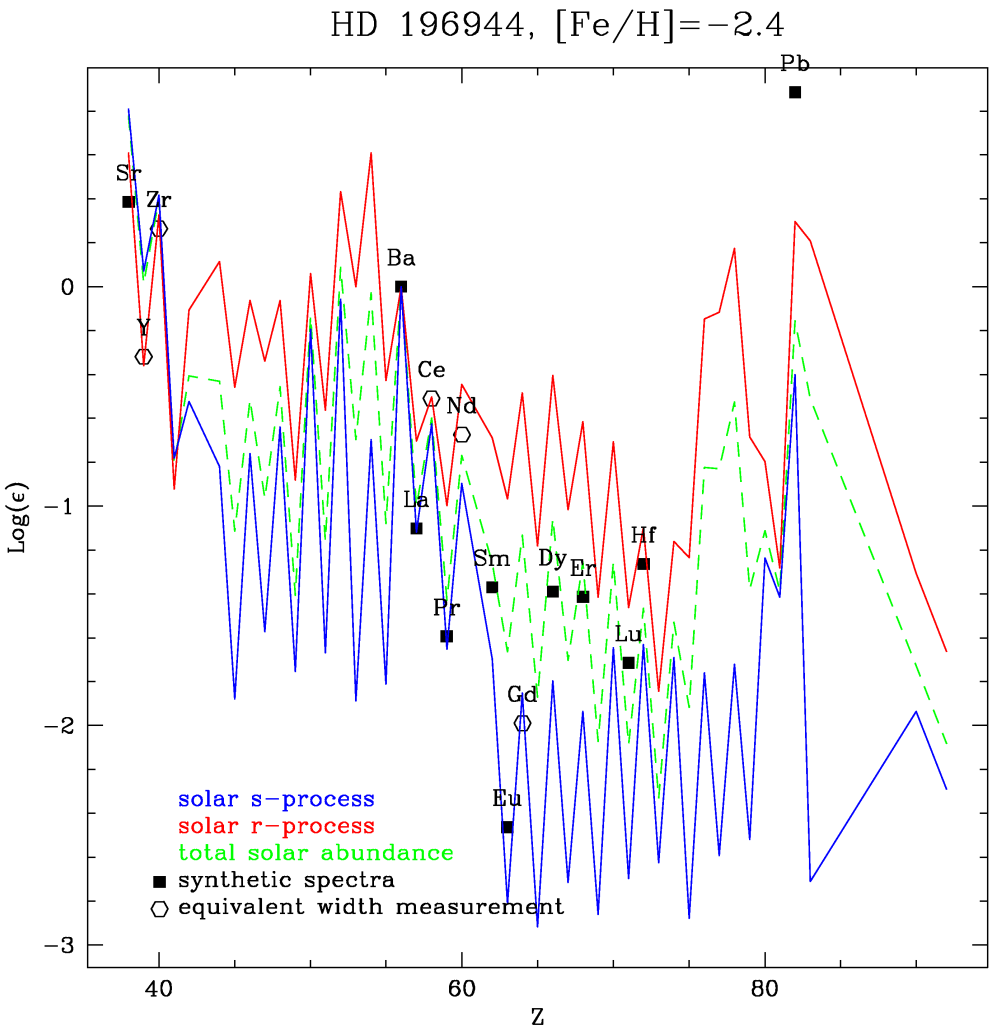


Fig. 7.—Scaled abundances in HD196944

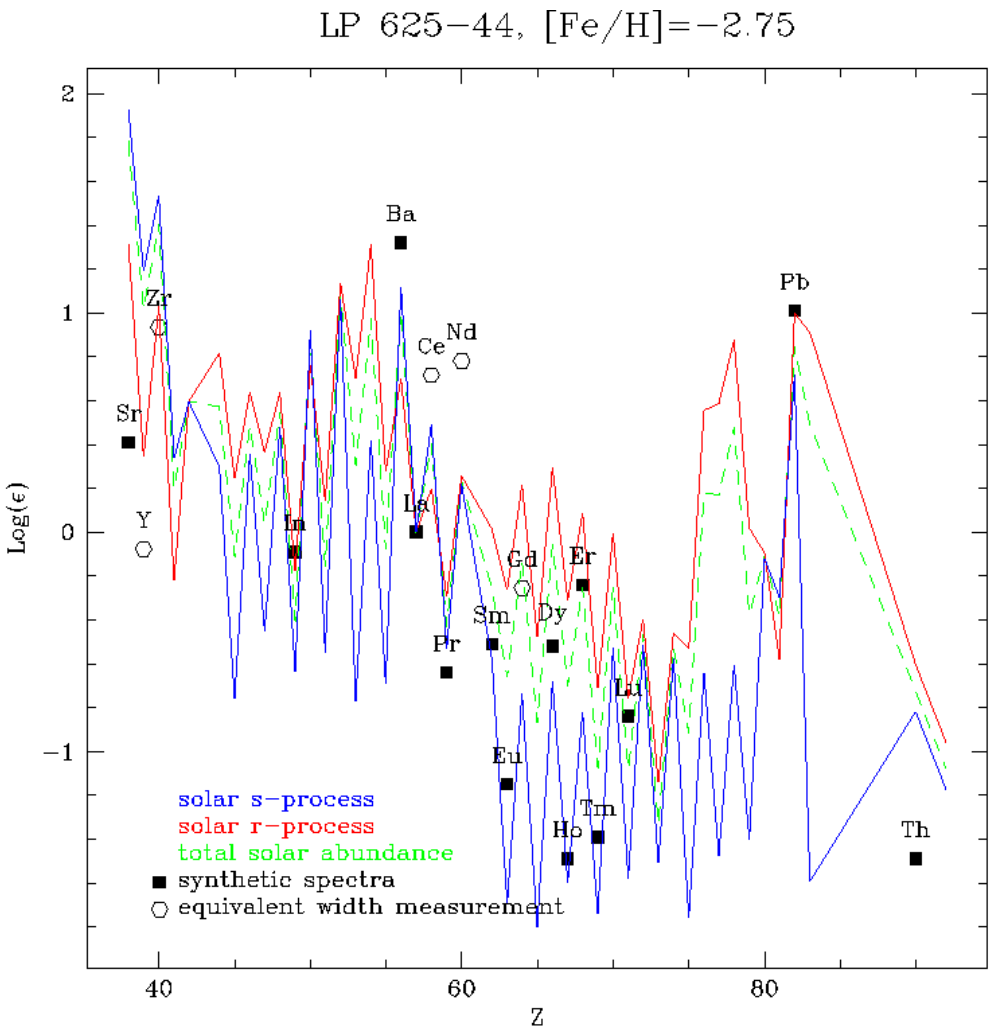


Fig. 8.—Scaled abundances in LP625-44

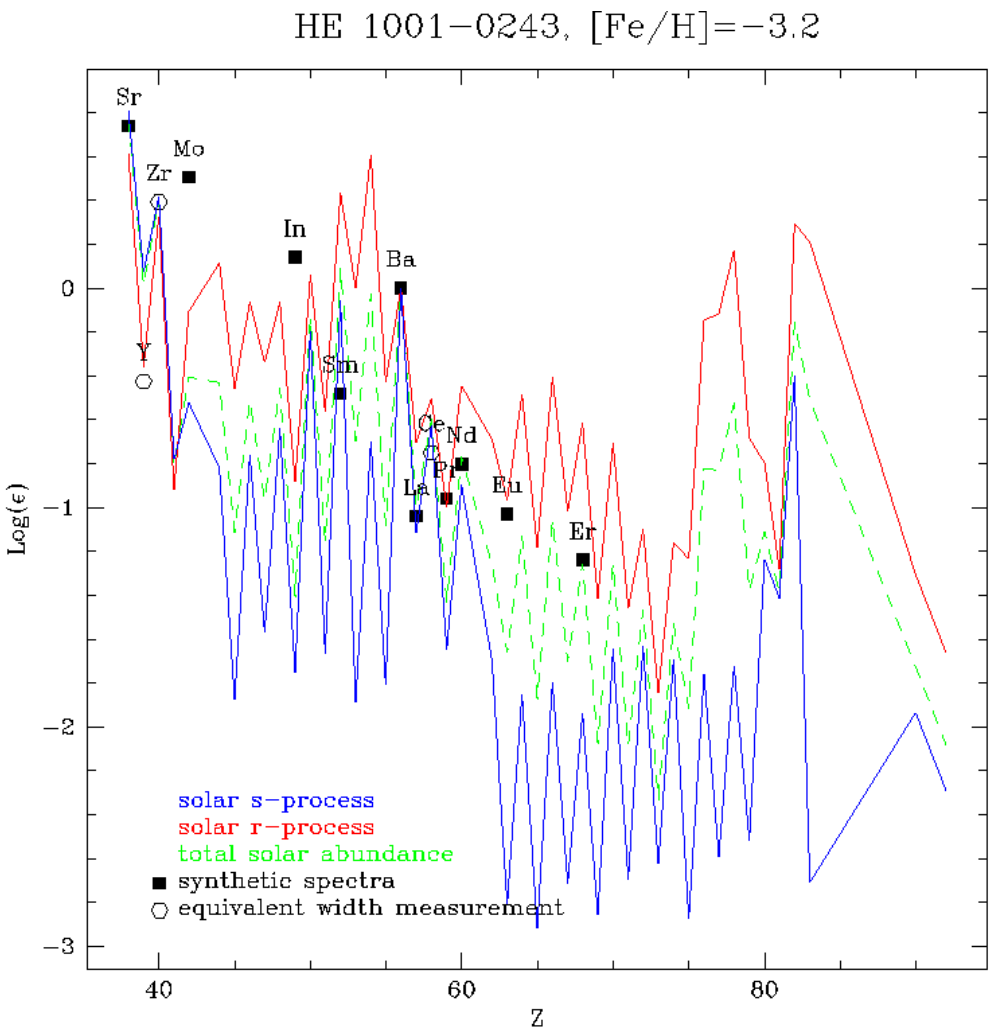


Fig. 9.—HE 1001-0243 shows signatures of both the s-process and r-process and would be classified as a CEMP-r/s star. The [Ba/Eu] ratio is indicative of an r-process enhancement, while the [Ba/La] ratio seems to fit an s-process pattern.

# 5. Data

## 5.1. Measured chemical abundances

| | BS 16080-175 | | CS 22877-001 | | G 64-12 | | HD 196944 | |
|---|---|---|---|---|---|---|---|---|
| element | $\log_\epsilon(X)$ | lines measured | $\log_\epsilon(X)$ | lines measured | $\log_\epsilon(X)$ | lines measured | $\log_\epsilon(X)$ | lines measured |
| Al | 3.73 | 1 | 2.19 | 1 | 2.40 | 2 | 3.34 | 1 |
| Ca | 4.98 | 28 | 3.36 | 17 | 3.36 | 8 | 4.34 | 25 |
| Cr 1 | 3.93 | 5 | 1.99 | 7 | 1.91 | 1 | 3.07 | 4 |
| Cr 2 | 4.22 | 7 | - - - | - - - | - - - | - - - | 3.44 | 10 |
| Fe 1 | 5.73 | 167 | 4.08 | 147 | 4.08 | 49 | 5.08 | 178 |
| Fe 2 | 5.74 | 13 | 4.13 | 8 | 4.08 | 2 | 5.08 | 13 |
| K | 3.82 | 1 | 2.03 | 1 | - - - | - - - | 3.22 | 1 |
| Mg | 5.94 | 9 | 4.44 | 9 | 4.50 | 5 | 5.57 | 7 |
| Mn | 3.70 | 7 | 1.76 | 3 | - - - | - - - | 2.97 | 10 |
| Na | 4.80 | 4 | 2.75 | 2 | 2.69 | 2 | 4.49 | 2 |
| Sc | 1.68 | 38 | -0.50 | 3 | -0.03 | 1 | 0.84 | 39 |
| Si 1 | 6.17 | 4 | 5.21 | 2 | 4.30 | 1 | 6.10 | 2 |
| Si 2 | 6.16 | 1 | - - - | - - - | - - - | - - - | 5.76 | 1 |
| Ti 1 | 3.62 | 7 | 1.52 | 4 | 2.23 | 10 | 2.91 | 20 |
| Ti 2 | 3.70 | 30 | 1.78 | 22 | - - - | - - - | 2.92 | 35 |
| V 1 | 3.42 | 3 | 1.63 | 3 | 3.20 | 1 | 1.51 | 1 |
| V 2 | 2.79 | 1 | - - - | - - - | - - - | - - - | 1.85 | 1 |
| | | | | | | | | |
| Ce | 1.48 | 10 | -1.72 | 1 | - - - | - - - | 0.20 | 10 |
| Gd | 0.43 | 1 | - - - | - - - | - - - | - - - | -1.28 | 1 |
| Nd | 1.29 | 13 | -1.88 | 1 | - - - | - - - | 0.04 | 15 |
| Y | 1.48 | 8 | -1.68 | 1 | - - - | - - - | 0.40 | 8 |
| Zr | 2.04 | 5 | -0.88 | 1 | - - - | - - - | 0.98 | 5 |
| Sr | 2.15 | syn. | -0.94 | syn. | -0.45 | syn. | 1.10 | syn. |
| Ba | 2.13 | syn. | -1.67 | syn. | -1.25 | syn. | 0.71 | syn. |
| La | 1.04 | syn. | -1.00 | syn. | - - - | - - - | -0.39 | syn. |
| Pr | 0.52 | syn. | - - - | - - - | - - - | - - - | -0.88 | syn. |
| Eu | -0.73 | syn. | -2.80 | syn. | - - - | - - - | -1.75 | syn. |
| Dy | 0.66 | syn. | -2.10 | syn. | - - - | - - - | -0.68 | syn. |
| Ho | -0.30 | syn. | - - - | - - - | - - - | - - - | - - - | - - - |
| Er | 0.53 | syn. | -1.67 | | - - - | - - - | -0.70 | syn. |
| Lu | - - - | - - - | - - - | - - - | - - - | - - - | -1.00 | syn. |
| Hf | 0.70 | syn. | - - - | - - - | - - - | - - - | -0.55 | syn. |
| Pb | 2.60 | syn. | - - - | - - - | - - - | - - - | 1.60 | syn. |

| | HE 1001-0243 | | HE 1005-1439 | | HE 1012-1540 | |
|---|---|---|---|---|---|---|
| | $\log_\epsilon(X)$ | lines measured | $\log_\epsilon(X)$ | lines measured | $\log_\epsilon(X)$ | lines measured |
| **Al** | 2.62 | 1 | 3.03 | 1 | 2.63 | 1 |
| **Ca** | 3.61 | 12 | 4.03 | 12 | 3.24 | 11 |
| **Cr 1** | 1.94 | 4 | 4.55 | 13 | 1.13 | 3 |
| **Cr 2** | - - - | - - - | 3.00 | 2 | - - - | - - - |
| **Fe 1** | 4.07 | 109 | 4.50 | 107 | 3.33 | 52 |
| **Fe 2** | 4.05 | 7 | 4.50 | 6 | 3.36 | 1 |
| **K** | 2.01 | 1 | 2.62 | 1 | - - - | - - - |
| **Mg** | 4.72 | 8 | 4.83 | 4 | 5.10 | 9 |
| **Mn** | 1.67 | 2 | 2.80 | 7 | 0.91 | 3 |
| **Na** | 3.72 | 2 | 4.31 | 2 | 3.62 | 2 |
| **Sc** | -0.08 | 2 | 0.82 | 3 | -0.32 | 1 |
| **Si 1** | 4.87 | 1 | - - - | - - - | 4.44 | 1 |
| **Si 2** | - - - | - - - | - - - | - - - | - - - | - - - |
| **Ti 1** | 1.87 | 5 | 2.89 | 4 | - - - | - - - |
| **Ti 2** | 2.07 | 23 | 2.53 | 14 | 1.36 | 8 |
| **V 1** | 2.25 | 3 | 2.65 | 2 | 2.29 | 5 |
| **V 2** | - - - | - - - | - - - | - - - | - - - | - - - |
| | | | | | | |
| **Ce** | -1.09 | 2 | -0.14 | syn. | - - - | - - - |
| **Gd** | - - - | - - - | -0.44 | syn. | - - - | - - - |
| **Nd** | -1.14 | syn. | -0.44 | 6 | - - - | - - - |
| **Y** | -0.77 | 3 | -0.33 | 1 | - - - | - - - |
| **Zr** | 0.05 | 3 | 0.21 | 5 | - - - | - - - |
| **Sr** | 0.40 | syn. | -0.25 | 2 | - - - | - - - |
| **In** | -0.20 | syn. | 0.60 | 1 | - - - | - - - |
| **Ba** | -0.34 | syn. | -0.08 | syn. | - - - | - - - |
| **La** | -1.38 | syn. | -1.43 | syn. | - - - | - - - |
| **Pr** | -1.30 | syn. | - - - | - - - | - - - | - - - |
| **Sm** | -0.82 | syn. | -1.29 | syn. | - - - | - - - |
| **Eu** | -1.37 | syn. | -2.44 | syn. | - - - | - - - |
| **Dy** | - - - | - - - | -1.00 | syn. | - - - | - - - |
| **Er** | -1.58 | syn. | - - - | - - - | - - - | - - - |

| | HE 1150-0428 | | HE 1419-1324 | | LP 625-44 | |
|---|---|---|---|---|---|---|
| element | $\log_\epsilon(X)$ | lines measured | $\log_\epsilon(X)$ | lines measured | $\log_\epsilon(X)$ | lines measured |
| Al | 3.06 | 1 | 2.78 | 1 | 3.49 | 1 |
| Ca | 4.11 | 6 | 3.67 | 11 | 4.21 | 15 |
| Cr 1 | 3.32 | 4 | 2.88 | 7 | 3.09 | 4 |
| Cr 2 | 3.91 | 1 | | | 3.96 | 2 |
| Fe 1 | 4.13 | 57 | 4.07 | 121 | 4.78 | 99 |
| Fe 2 | 4.13 | 2 | 4.08 | 6 | 4.77 | 6 |
| K | - - - | - - - | - - - | - - - | 2.76 | 1 |
| Mg | 4.42 | 2 | 4.76 | 8 | 5.69 | 7 |
| Mn | 2.23 | 2 | 2.52 | 4 | 3.47 | 7 |
| Na | 4.27 | 2 | 3.97 | 2 | 5.28 | 7 |
| Sc | 1.26 | 1 | -0.36 | 35 | 1.31 | 3 |
| Si 1 | - - - | - - - | - - - | - - - | 6.72 | 1 |
| Si 2 | - - - | - - - | - - - | - - - | - - - | - - - |
| Ti 1 | 3.29 | 2 | 1.71 | 6 | 3.54 | 6 |
| Ti 2 | 2.30 | 10 | 1.85 | 15 | 2.75 | 15 |
| V 1 | 3.17 | 5 | 3.09 | 2 | - - - | - - - |
| V 2 | - - - | - - - | - - - | - - - | - - - | - - - |
| | | | | | | |
| Ce | -0.19 | 2 | -1.02 | 3 | 1.81 | 9 |
| Gd | - - - | - - - | -1.54 | 1 | 0.83 | 1 |
| Nd | 0.10 | syn. | -0.94 | 6 | 1.87 | 15 |
| Y | -0.67 | syn. | -1.37 | 1 | 1.01 | 5 |
| Zr | 0.80 | syn. | -0.70 | 1 | 2.03 | 4 |
| Sr | -0.40 | syn. | -1.10 | syn. | 1.50 | syn. |
| In | - - - | - - - | - - - | - - - | 1.00 | syn. |
| Mo | - - - | - - - | -0.30 | syn. | - - - | - - - |
| Ba | -1.87 | syn. | -0.17 | syn. | 2.41 | syn. |
| La | 0.27 | syn. | -1.14 | syn. | 1.09 | syn. |
| Pr | 0.30 | syn. | -1.90 | syn. | 0.45 | syn. |
| Sm | 0.12 | syn. | -1.37 | syn. | 0.58 | syn. |
| Eu | -1.20 | syn. | -2.53 | syn. | -0.06 | syn. |
| Dy | - - - | - - - | -1.88 | syn. | 0.57 | syn. |
| Ho | - - - | - - - | - - - | - - - | -0.40 | syn. |
| Er | - - - | - - - | -1.51 | syn. | 0.85 | syn. |
| Tm | - - - | - - - | - - - | - - - | -0.30 | syn. |
| Lu | - - - | - - - | - - - | - - - | 0.25 | syn. |
| Pb | - - - | - - - | - - - | - - - | 2.10 | syn. |
| Th | - - - | - - - | - - - | - - - | -0.40 | syn. |

### 5.2. Carbon enhanced vs. non-enhanced models

| | Δ Abundance (dex), C-enriched - normal models | | |
|---|---|---|---|
| element | BS 16080-175 | HD 196944 | HE 1150-0428 |
| Al | 0.03 | 0.03 | 0.07 |
| Ca | 0.02 | 0.03 | 0.06 |
| Cr 1 | 0.03 | 0.04 | 0.07 |
| Cr 2 | 0.00 | 0.00 | 0.01 |
| Fe 1 | 0.03 | 0.03 | 0.07 |
| Fe 2 | 0.01 | 0.01 | 0.02 |
| K | 0.02 | 0.03 | - - - |
| Mg | 0.03 | 0.03 | 0.06 |
| Mn | 0.03 | 0.03 | 0.07 |
| Na | 0.02 | 0.03 | 0.05 |
| Sc | 0.01 | 0.02 | 0.02 |
| Si 1 | 0.02 | 0.03 | - - - |
| Si 2 | -0.02 | -0.01 | - - - |
| Ti 1 | 0.03 | 0.03 | 0.08 |
| Ti 2 | 0.01 | 0.02 | 0.04 |
| V 1 | 0.03 | 0.03 | 0.07 |
| V 2 | 0.01 | 0.01 | - - - |

### 5.3. Lithium abundances and upper limits

| Star | Li abundance (dex) | Upper limit on Li (dex) |
|---|---|---|
| BS 16080-175 | - - - | 1.20 |
| CS 22877-001 | 0.55 | - - - |
| G 64-12 | 2.15 | - - - |
| HD 196944 | - - - | 0.0 |
| HE 1001-0243 | - - - | 0.4 |
| HE 1005-1439 | - - - | 0.0 |
| HE 1012-0428 | - - - | 0.0 |
| HE 1150-0428 | - - - | 0.0 |
| HE 1419-1324 | - - - | -0.5 |
| LP 625-44 | - - - | 0.0 |

# 6. Appendices

## 6.1. Metallicity

The metallicity of a star is often expressed as the logarithmic ratio [Fe/H], which is a comparison of its iron abundance to that of the Sun. Iron is used in this definition not because it is the most abundant metal, but because it is easily measured in the visible range of the spectrum.

$$\left[\frac{Fe}{H}\right] = Log\left(\frac{N_{Fe}}{N_H}\right)_{star} - Log\left(\frac{N_{Fe}}{N_H}\right)_{Sun} \tag{1}$$

where $N_{Fe}/N_H$ is the ratio of the number of iron/hydrogen atoms in the star and the sun. By this definition, a star with the same metal content as the Sun (1.8% by mass) has [Fe/H] = 0. A star is considered to be metal-poor if it has a value of [Fe/H] < -1.0, which corresponds to a metal content less than one-tenth that of the Sun. The units of metallicity are referred to as 'dex, short for 'decimal exponent.

Iron abundance is used to describe metallicity primarily because its absorption lines are easiest to measure in the visible portion of a stellar spectrum. The abundances of other metals in a star (such as carbon or oxygen) relative to its hydrogen abundance often differ from its iron-to-hydrogen ratio. Differences in elemental proportions are also quantified by comparing them to the ratios in the Sun, for example:

$$\begin{aligned}\left[\frac{X}{Fe}\right] &= Log\left(\frac{N_X}{N_{Fe}}\right)_{star} - Log\left(\frac{N_X}{N_{Fe}}\right)_{Sun} \\ &= \left[Log\left(\frac{N_X}{N_H}\right)_{star} - Log\left(\frac{N_X}{N_H}\right)_{Sun}\right] - \left[Log\left(\frac{N_{Fe}}{N_H}\right)_{star} - Log\left(\frac{N_{Fe}}{N_H}\right)_{Sun}\right]\end{aligned} \tag{2}$$

Elemental abundances can also be described without referencing the solar abundance. Abundances on this absolute scale are relative to the number of hydrogen atoms and are given by

$$Log_\epsilon(X) = Log\left(\frac{N_X}{N_H}\right) + 12.0 \tag{3}$$

### 6.2. Measurement of equivalent widths

Equivalent width is the measure used to compare the strengths of different absorption lines. The formal expression is given by equation 4. The interpretation of this formula is that equivalent width is the width (usually given in mÅ) of a rectangle with the same height of the spectral continuum and the same area as the line in question.

$$\int_{\lambda_1}^{\lambda_2} \frac{f_{cont} - f_\lambda}{f_{cont}} d\lambda \tag{4}$$

Spectral line are not perfectly sharp- they have finite widths that are mainly a result of thermal and natural broadening. Atomic energy levels are intrinsically broadened due to the uncertainty principle, which leads to natural broadening since line wavelengths are determined by the energy difference in atomic energy level transitions. This type of broadening creates a Lorentzian, or damping profile. Thermal motions of gas Doppler shift lines, creating a Gaussian line profile. The observed absorption line is a convolution of these two profiles, known as a Voight profile. The Gaussian dominates in the core, while the damping decay dominates in the wings. However, the Doppler core is very wide compared to the Lorentzian, so the damping wings are only observable in very strong lines. Therefore in almost all cases, the area of an absorption line can be found be fitting a Gaussian function to it and then integrating.

## REFERENCES

Alverez, R. & Plez, B. 1998, A&A, 330, 1109
Aoki, W. et al, 2002, ApJ, 580, 1149
Barlow, T. 2002 MAKEE Keck Observatory HIRES Data Reduction Software,
http://spider.ipac.caltech.edu/staA/tab/makee
Beers, T. & Christlieb, N. 2005, ARA&A, 43, 531
Beers, T., Preston, G., & Schectman, S. 1992, ApJ, 103, 1987
Busso, M. Gallino, R. & Wasserburg, J. 1999, ARA&A, 37, 239
Cohen, J. et al. 2006, AJ, 132, 137
Fitzpatrick, M.J. & Sneden, C. 1987, BAAS, 19, 1129
Fujimoto, M., Ikeda, Y. & Iben, I. 2000, ApJ, 529, L25
Gustafsson, B., et al. 2008, A&A, 486, 951
Goriely, S. & Mowlavi, N., A&A, 362, 599
Ivans, I. et al. 2005, ApJ, 625, L145
Lucatello, S. et al. 2005, ApJ, 625, 825
Lucatello, S. et al. 2006, ApJ, 652, L37
Lugaro, M., Campbell, S. & deMink, S. 2009, PASA, 26, 322
Masseron, T. et al. 2010, A&A, 509, A93
Moore, C. E., Minnaert, M. G. J., & Houtgast, J. 1966, The solar spectrum 2935Åto 8770Å
Norris, J., Ryan, S., & Beers, T.1997, ApJ, 488, 350
Ramirez, I. & Melendez, J. 2005, ApJ, 626, 425
Vogt, S. et al. 1994, SPIE, 2198, 362
Wanajo, S. et al. 2006, ApJ, 636, 842